GUIDANCE AND CONTROL SYSTEM RESEARCH FOR IMPROVED TERMINAL AREA OPERATIONS*

R. M. Hueschen, J. F. Creedon, W. T. Bundick, and J. C. Young

NASA Langley Research Center

ABSTRACT

Several guidance and control system research and development activities aimed at improving the operational capabilities of commercial aircraft in the terminal area are described. The guidance and control systems have been designed to improve the capacity and efficiency of terminal area operations, enhance the approach and landing capability of aircraft in adverse weather conditions, and reduce the impact of aircraft noise perceived on the ground. Specific performance features include the ability to capture and track steep glideslopes, use short final approaches, perform flares with reduced longitudinal touchdown dispersion and execute high speed runway rollout and turnoff. Results obtained from simulation studies or flight tests are shown for each of the algorithms.

INTRODUCTION

Significant improvements in the terminal area operational capability of commercial aircraft are being sought to alleviate crowded conditions at major airports and to enhance safety and schedule reliability. The Terminal Configured Vehicle (TCV) program being pursued at Langley Research Center has the goal of providing flight management and CTOL aircraft technology to increase terminal area capacity and efficiency, to improve the approach and landing capability of aircraft operating in adverse weather conditions, and to reduce the aircraft-generated noise perceived on the ground. This paper presents some results obtained from a coordinated guidance and control system development effort directed to support the TCV program.

---

* The work presented comprises the results of both in-house and contractual research efforts. In particular, the DIALS design effort was performed by Dr. N. Halyo currently of the Information and Control Systems, Inc.; two flare law algorithms were developed by A. A. Lambregts of the Boeing Co.; and the initial rollout and turnoff guidance and control law was developed by S. Pines of the Analytical Mechanics Associates, Inc.

Automatic guidance and control systems are presented for glideslope and localizer capture and track, flare and landing, rollout, and runway exit. For all flight phases considered, the aircraft sensors providing acceleration, attitude, altitude, and body rate data are augmented by information derived from the Time Referenced Scanning Beam Microwave Landing System (MLS) under development by the FAA. The MLS consists of a precision DME providing range information and discrete azimuth and elevation signals available within the specified volumetric coverage. In cooperative efforts between NASA and the FAA, many automatic approaches and landings have been performed by the TCV B-737 aircraft to demonstrate the utility of this information in flying curved approaches to relatively short finals (refs. 1, 2, 3, 4, and 5). To enhance and extend the autoland capability and performance levels previously demonstrated, a digital, integrated automatic landing system (DIALS) has been developed using a modern control theoretic approach. The DIALS algorithm provides rapid capture and precise tracking of glideslope and localizer--including the capability of simultaneously performing both capture maneuvers. This feature enhances the efficient use of terminal area airspace by permitting aircraft to be flown along separate curved approach paths and merged only for short final approaches. The control law also permits tracking of pilot selectable steep glideslopes. The lower thrust levels required for steep glideslopes reduce the noise emanating from the aircraft and the greater attenuation afforded by the increased altitudes further reduces the noise levels perceived on the ground. To improve passenger comfort and control performance in adverse weather conditions, the DIALS algorithm generates estimates of wind velocities and uses these estimates in the control loop.

Several research efforts were pursued to increase runway landing capacity by reducing the time each aircraft occupies the runway. To limit the occupancy time, each inbound aircraft would flare to a landing at a prescribed distance from the desired exit. The aircraft would then be automatically controlled to follow a closed-loop deceleration program during rollout and perform a high speed turnoff. Reduction of the longitudinal touchdown footprint is essential since short landings requiring large occupancy times or long landings resulting in missed turnoffs would disrupt the flow of traffic and decrease the landing rate achieved. To obtain improved flare performance, two algorithms were developed and flight tested. The first flare law commands altitude as a function of sink rate to achieve an exponential path. The time constant is varied as a function of ground speed to ameliorate the effect of variations in ground speed on touchdown location. The second flare algorithm commands the aircraft to follow an explicitly defined path-in-space. This approach has the potential to further reduce touchdown dispersions by also minimizing the effects of glideslope tracking errors on touchdown location.

To extend automatic operations through rollout and turnoff, the aircraft is commanded to follow a prescribed path. The path is defined by a magnetic leader cable imbedded in the runway and turnoff. Signals obtained from a three coil magnetic sensor mounted on the aircraft are processed to yield measurements of the aircraft's heading and lateral deviation from the desired path. These measurements are used in a rollout and turnoff guidance and control law which provides deceleration and steering commands for both wet and dry runway conditions.

In the subsequent sections, descriptions are given of each of the control algorithms and results are given for simulation, prototype evaluation or flight testing. The DIALS design philosophy and performance advantages are discussed. Results of detailed simulation studies are given to demonstrate significantly improved performance relative to existing autoland system designs. The flare algorithms are described and the effect of the design concepts on touchdown dispersion is illustrated. Results of extensive flight tests of the flare laws are reviewed. Both theoretical and field test results for the magnetic leader cable and the associated sensor are presented. The deceleration program is given along with rollout and turnoff guidance and control performance results obtained from a simulation study using a detailed model of the sensor derived from the field tests.

DIALS

Current operational autoland systems perform well the task they were designed to accomplish. However, increased capabilities are being demanded for autoland systems to solve some of the problems of the increasingly crowded terminal area airspace. These demands include improved performance in adverse weather conditions, tracking of steep and selectable glideslopes for noise reduction, avoidance of wake vortices, and reduced fuel consumption. The current systems have limitations which make it impossible for them to meet the demands for increased capabilities. The DIALS design was undertaken to provide a system with expanded capabilities free of the current limitations. The DIALS is a complete software algorithm designed and developed for the automatic landing of a commercial type aircraft. The tasks performed by the DIALS (see figure 1) are: (1) close-in simultaneous capture of the localizer and glideslope including steep glideslopes up to 6 degrees, (2) tracking of the localizer and glideslope, (3) a sideslip decrab maneuver (the same type decrab maneuver performed manually by pilots), (4) the flare maneuver from the various selected glideslopes, (5) precision touchdown, (6) calibrated airspeed (CAS) hold, (7) stabilizer trim, and (8) inner loop damping including the yaw rate damper function. First, some of the limitations of the current systems will be given and then the approach and methods used in the design of the DIALS will be presented.

The current autoland systems use the Instrument Landing System (ILS) for guidance along the localizer and glideslope paths. The ILS restricts guidance to one fixed glideslope and also often has characteristic beam bends on the localizer signal. In addition, these systems use the classical approach to control system design in which the gains are determined through root locus techniques and specified gain and phase margin criteria. These techniques can be applied only to single-input single-output portions of the system--a limitation of the classical approach. Thus after the initial determination the gains must be adjusted by trial and error procedures to account for the interaction between the multiple inputs and outputs of the system. One final point to be made concerning the present systems is that the systems are analog. Special programming efforts and analyses are generally required to implement an analog system on a digital computer.

The DIALS differs from systems currently being flown in several ways. First, it was designed to use the MLS rather than the ILS. The MLS provides the information necessary to fly different glideslopes as well as providing signals relatively free of beam bends (multipath effects). Second, the system was designed using modern digital control theory techniques and methods as opposed to the classical approach. The modern control theory approach provides a means for defining the total system and control requirements within a unified set of equations. Then from the total set of equations all the system feedback gains are mathematically determined simultaneously. The simultaneous solution of the gains is referred to as an integrated design--the second character of the DIALS acronym. For DIALS this method was applied once to a unified set of lateral system equations and then to a set of longitudinal equations (refs. 6, 7, and 8). The integrated design results in commands coordinated among the longitudinal controls as well as commands coordinated between the lateral controls. For instance, if a reduction in airspeed is desired while maintaining glideslope track, DIALS will produce coordinated throttle and elevator commands. The throttle reduction will be accompanied by an elevator command calling for a pitch up to maintain the glideslope track (reduced airspeed results in reduced lift and subsequent movement below the glideslope).

Another feature of the DIALS is that it is a digital or discrete design--the first character of the acronym. This means that the differential equations describing the system were discretized into a system of difference equations. The difference equations were then used in the modern control theory approach to determine the system control gains and the filter gains for estimating the state variables of the system from one sampling instant to the next. The digital design results in a set of difference equations for updating the guidance and control commands and a set for updating the filter equations.

There were several reasons for choosing a digital design. First, aircraft avionics technology is moving toward the use of digital flight control computers and the control laws would ultimately be discretized anyway for implementation on the flight computer. Second, the MLS system used by DIALS provides the aircraft's position at discrete intervals of time rather than continuously. Also, the aircraft sensor measurements will only be available at discrete sampling instants on a digital computer. For these reasons, a digital design was chosen for the DIALS.

A feature of the digital design is that the update interval or rate of the flight control computer is specified in the formulation of the set of system difference equations. This results then in a set of control system gains which take into account the update rate of the computer. Another important feature of the DIALS design is that the continuous cost function (the means of weighing the control law performance in the modern control theory design) was discretized in a manner such that the system dynamics between sampling instants is included in the discrete cost function (ref. 6). The inclusion of the system dynamics between sampling instants makes it possible to use larger sampling intervals than generally used. Thus the real-time computational requirements on the flight control computer are reduced. For the DIALS the update rate is 10 times per second.

The DIALS consists of three basic functions--navigation/filtering, guidance, and control about a desired path. (The relationship of these functions is illustrated in figure 2.) The navigation/filtering function estimates the aircraft position and other parameters using a steady-state Kalman filter, that is, a Kalman filter whose gains remain constant for a given approach and landing. The filter determines the aircraft position in a runway coordinate frame using aircraft sensors and measurements of azimuth, elevation, and range from the MLS. The filter also provides estimates of the aircraft attitude, velocity, accelerometer biases, barometric altitude and barometric sink rate biases, and wind velocities. The DIALS was also formulated to take into account the effects of wind disturbances on the aircraft. The wind states were weighed in the discrete cost function and thus the control commands are a function of the wind state estimates. Wind velocity estimates are provided for the steady state, gust, and shear wind components. The aircraft sensor measurements used by the filter are attitudes, attitude rates, body-referenced accelerations, barometric altitude and sink rate, radar altitude, and calibrated airspeed.

The guidance function determines the tracking errors from the desired flight path (trajectory) using the aircraft state and wind estimates. The generation of the desired flight path, which was formulated to be a function of several selectable parameters, is also part of the guidance function. Pilot selectable parameters include the desired glideslope angle and the calibrated airspeed. Other parameters which can be changed to tailor the flare trajectory are the glide path intercept point (GPIP), the touchdown point, touchdown sink rate, and the airspeed reduction during flare. The control function determines the control commands necessary (1) to null the errors or deviations from the commanded trajectory, (2) to maintain aircraft trim, and (3) to damp the inherent natural frequency modes of the aircraft (inner loop damping). The commands computed are elevator and aileron position and rudder, stabilizer, and throttle rate. The stabilizer rate commands are converted through logic equations to trim up and trim down discretes to interface with the aircraft's stabilizer trim motor.

The use of rate commands provided a means for formulating an automatic trim capability into the control law. By using rate commands no penalty is incurred on position changes, but only on excessive rates of change. Aileron and elevator position commands were used to provide quickness of response. Also, the use of position commands in the cost function prevents large stand-off position commands which could result in large undesirable hinge-moments for these control surfaces.

The control commands are functions of the aircraft states, wind velocities, nominal flight path, and commanded path deviations from the nominal flight path as illustrated in figure 3. The nominal trajectory or flight path consists of the straight line localizer and glideslope path as well as the nominal aircraft state. Deviations from the nominal trajectory are commanded during the decrab and flare maneuvers.

The DIALS has been tested via a digital computer simulation which used a six degree of freedom non-linear model of the TCV B-737 aircraft. The simulation included sensor noises and biases, such as accelerometer misalignment and scaling errors, and various wind conditions--steady state, gust, and shear. The servos were modeled as first order lags.

Simulation results are shown in figures 4 and 5. Figure 4 compares the capture and track of the localizer with the current TCV B-737 localizer capture and track algorithm. It can be seen that the DIALS capture occurs within 40 seconds as opposed to the 120 seconds or so for the current algorithm. This capability to fly short final approach paths is important for efficient air traffic control operations. Also note that the overshoot performance is much lower for DIALS. This performance, which has been demonstrated for various simulated wind conditions, is important in achieving reduced runway spacing for parallel runway operations. The sideslip decrab maneuver is also illustrated in the roll and yaw plots. Figure 5 compares the capture of a six degree glideslope by DIALS with the capture of a three degree glideslope by the TCV B-737 ILS glideslope capture algorithm. Note that the capture and settling time for DIALS is 5 seconds while at least 30 seconds is required for the TCV B-737 algorithm. It is also noted that this capture occurred simultaneously with the localizer capture. Simultaneous capture is important because it contributes to reducing the length of the final approach path. However, the DIALS can perform the captures independently. The capability to fly various glideslope angles, including steep final approaches, provides the means for noise reduction along the ground track and avoidance of trailing vortices.

FLARE LAW DEVELOPMENT

Certification under FAA AC 20-57A for commercial aircraft requires automatic landing systems to meet a $\pm 2\sigma$ longitudinal touchdown dispersion of 457.2 m (1500 ft). Flare laws which provide touchdown dispersions smaller than this requirement are desirable for several reasons. The precise flare performance can be combined with a capability to perform high-speed exits and thus increase runway landing capacity by limiting runway occupancy time. In addition, reduction in touchdown dispersion is an effective means of reducing the operational field length requirement. The TCV program has established a longitudinal touchdown dispersion criterion of $1\sigma \leq 30.5$ m (100 ft) as being commensurate with their specific goals for improved terminal area performance. To attain this goal, factors contributing to touchdown dispersion have been evaluated and several flare concepts have been identified to ameliorate the effects of specific sources of dispersion.

Many flare laws in current use command sink rate as a function of altitude. Algorithms of this type, designated here as $\dot{h}$ (h) flare laws, are designed to provide an exponential flare path. To obtain transient-free initiation the flare is started at the altitude at which the commanded flare sink rate becomes equal to the measured sink rate. The TCV B-737 used a flare law of this type during autoland demonstrations performed for the ICAO all-weather operations panel at the FAA's National Aviation Facilities Experimental Center

(NAFEC) in May 1976 (refs. 1 and 2). The touchdown performance for 56 landings performed during this demonstration was:

Longitudinal dispersion (1σ) = 94.2 meters (309 ft)

Sink rate (mean/1σ) = .713/.430 m/sec (2.34 / 1.41 ft/sec)

This performance was achieved with average wind velocities of 8.23-10.29 meters/sec (16-20 knots) and relatively large gusts and tail winds (ref. 1). While the longitudinal dispersion was better than the FAA requirement, it fell short of the TCV goal. Accordingly, a detailed study, to be described in a contractor report, was performed by the Boeing Company to identify factors which contribute to touchdown dispersion. Flare law designs were then sought to reduce their effects. One such factor is that approaches in different steady wind conditions are performed at different ground speeds; consequently, the flare initiation altitude and touchdown point can vary significantly. Figure 6 shows a variation of over 152.4 meters (500 ft) in touchdown location for approaches flown at $V_{ref.}$ + 2.57 meters/sec (5 knots) in steady wind conditions ranging from a 12.86 meters/sec (25 knots) headwind to a 7.72 meters/sec (15 knot) tail wind. These results were obtained from a simulation of the TCV B-737 for an $\dot{h}$ (h) flare law of the type used during TCV autoland demonstrations. It is noted that the flare initiation altitude varies by over six meters during these conditions--a variation which increases the difficulty experienced by pilots in monitoring flare performance. Glideslope tracking errors and errors in the estimates of aircraft sink rate can also make significant contributions to touchdown dispersion. To reduce longitudinal touchdown dispersions, two flare concepts have been developed and evaluated. The concepts, called the variable time constant flare law and the fixed-path flare laws, are described in the following sections.

Variable Time Constant Flare Law

Figure 6 illustrates the effect on flare performance of variations in approach speed to accommodate steady wind conditions. To reduce the resulting dispersion, several approaches were investigated. In the selected approach, the time constant (ratio of the control gain on sink rate to the gain on altitude) is defined as

$$T = \frac{T_o \quad V_{Go}}{V_G} \qquad (1)$$

where T is the time constant, V_{Go} is the nominal approach ground speed and V_G is the actual approach ground speed. This modification provides transient free initiation at a fixed altitude--chosen as 12.8 m (42 ft) during this study. Simulation results for this algorithm are shown in figure 7 for the various head wind/tail wind conditions used in the simulation illustrated in figure 6. These results confirm the ability of this flare law, designated as the $\dot{h}$ (h, V_G) or

variable time constant flare law, to eliminate the effects of steady winds on touchdown dispersion. Prior to flight evaluation, an improved inner loop was designed and the $\dot{h}$ signal was developed as the output of a first order complementary filter using vertical acceleration from the INS and altitude from the radar altimeter. Selection of 12.8 m as the flare initiation altitude, insures that the aircraft will be over the runway at most airports and the radar altimeter signal will not be affected by uneven approach terrain during the flare. In production configurations the $\dot{h}$ signal derivation would be made an implicit function of the $\ddot{h}$, $\dot{\theta}$ inner loop filter. Implicit h derivation and initialization of the filter at the time of flare avoids carrying pre-flare terrain history, stored on the complementary filter, into the flare.

Flight evaluation of the $\dot{h}$ (h, V_G) flare law was performed using the TCV B-737 aircraft and the associated experimental system (ref. 9). The flare algorithm was implemented in the triple channel fail-operational flight control computers which computed flare commands at 20 iterations/second and performance data was obtained during automatic landing demonstrations performed at Dorval Airport in Montreal, Canada during 1978. During the demonstrations, flare data was obtained for 58 landings on 10 days while carrying passengers connected with an ICAO All-Weather Operations Division meeting. Several equipment configurations were used; however, over the last 40 runs both the equipment and system configuration were unchanged. A summary of the flare law performance at touchdown for these runs is:

Longitudinal dispersion (1σ) = 41.8m (137 ft)

Sink rate (mean/1σ) = .87/.19 m/sec (2.84 / .62 ft/sec)

All touchdowns were located in a 196 m (641 ft) range. This compares very favorably with 1500 ft (457.2 m) FAA $\pm$ 2σ footprint requirement and indicates that the flare law did not experience any extremely short or long landings. A more detailed discussion of both the flare design concept and flight test performance is contained in reference 10.

Fixed-Path Flare Law

A second approach to reducing touchdown dispersion involves commanding the aircraft to fly a fixed flare trajectory that is explicitly defined as a function of runway distance. Flares of this type, designated path-in-space or h(x) flare laws, have several advantages. The path is unchanged for variations in approach speed. The explicitly defined path may be altered independently of the gains used to achieve damping and turbulence response. Conversely the effects of feedback gains can be studied without changing the flare path. When an estimate of aircraft position is available such as can be provided by MLS, the flare is initiated at a preselected value of x and the path may be made a continuous extension of the glide path. This approach would enable the flare law to reduce the effect of glideslope tracking errors at flare initiation on touchdown location. Finally, commands for h (x), $\dot{h}$ (x), and $\ddot{h}$(x) can be developed to provide close tracking of the desired trajectory.

Two path-in-space trajectories have been studied. The first, designed for use with a nominal 3^{o} glideslope, specifies the first path as:

$$h_c(x) = \frac{K_1}{K_2^2} e^{-K_2 x} - \frac{K_1}{4K_2^2} e^{-2K_2 x} + K_3 x + K_4 \qquad (2)$$

The four constants K_1 through K_4 were chosen to satisfy the boundary conditions

$$\dot{h}_1 = \dot{h}_{GLIDE\ PATH} \quad \text{at flare initiation} \qquad (3)$$

$$h_1 = 12.8\ m\ (42\ ft) \qquad (4)$$

$$\dot{h} = \dot{h}_{DESIGN\ VALUE} \quad \text{at touchdown} \qquad (5)$$

$$x = x_{DESIGN} \qquad (6)$$

The corresponding $\dot{h}_1$ and $\ddot{h}_1$ commands are developed by differentiating the $h_1(x)$ command and dropping terms involving $\ddot{x}$. This formulation provides transient free flare initiation at fixed altitude for fixed glideslope approaches as well as specifying a gradual increase of $\ddot{h}_1$ to a maximum followed by a smooth reduction. Figure 8 shows the $h_1(x)$ trajectory for the aircraft dynamics and wind conditions used in generating figures 6 and 7.

The $h_1(x)$ flare law was evaluated during 1978 at NAFEC. For these tests the value of x was obtained from MLS measurements as described in reference 2. MLS configurations both with and without the flare elevation antenna were used. Performance was better with the flare elevation antenna--primarily as a result of onboard processing resolution. With the flare elevation antenna, 32 runs were made with touchdown performance of

Longitudinal dispersion (1σ) = 28.0 meters (92 ft)

Sink rate (mean/1σ) = .78 / .16 m/sec (2.56 / .51 ft/sec)

All flares which can be logically grouped together are summarized even though during the first part of the h(x) test program, several minor configuration changes were made. The performance during the latter portion of the testing, in which the configuration was held constant, indicates that the system was improved by these changes. For example, the last 18 landings using guidance derived from the flare elevation antenna were performed with a constant configuration. For these landings, a longitudinal dispersion of 48.3 ft was obtained with no degradation in the mean and standard deviation of touchdown sink rate.

This fixed-path flare concept was also evaluated in an ILS mode. When using the ILS the aircraft's position is not known; consequently, the flare was initiated at a radar altimeter reading of 12.8 m. The value of x required to generate $h_1(x)$, $\dot{h}_1(x)$ and $\ddot{h}_1(x)$ was obtained by integrating ground speed from the INS. For this configuration 23 runs were made resulting in

Flare distance (1σ) = 28.7 m (94 ft)

Sink rate (mean/1σ) = .71/.15 m/sec (2.33 / .50 ft/sec)

The variation in flare distance does not represent the total variation in touchdown position since errors in glideslope tracking at flare affect only the latter. Other flight tests with this aircraft indicated that the 1σ longitudinal dispersion attributable to glideslope tracking errors is 14.9 m (49 ft). This value was combined in an RSS manner with the 1σ value for flare distance to obtain an estimate of 32.3 m (106 ft) (1σ) in touchdown position.

An alternative h(x) formulation has been developed to accommodate the DIALS approaches which have selectable, steep-glideslope capability. In this approach $\ddot{h}_2(x)$ was specified as a 1-Cosine function. The $\dot{h}_2(x)$ and $h_2(x)$ commands were obtained though expressions formulated from off line integration of the $\ddot{h}_2(x)$ function. Constants are selected to provide transient free initiation for the glideslope being flown and to achieve the specified touchdown point and flight path angle. The flare initiation altitude is determined on line as a function of the selected glide path and specified touchdown parameters.

Simulation studies have been performed to evaluate the performance of this flare law. The studies used a nonlinear aircraft model and included sensor noise and atmospheric disturbances. The touchdown performance obtained for twenty flares from a 6° glideslope was

Longitudinal dispersion (1σ) = 34.4 m (113 ft)

Sink Rate (mean/1σ) = .66/.26 m/sec (2.18 / .85 ft/sec)

A graphical presentation of the performance results for the $h_1(x)$ fixed path and $\dot{h}(h, V_G)$ flare law is shown in figure 9. This figure also contains the performance of the baseline $\dot{h}(h)$ flare law.

In summary, both the variable time constant and specified trajectory laws can achieve significant reductions in longitudinal touchdown dispersion with reasonable values for the mean and standard deviation of touchdown sink rate. The flare laws performed well using currently available guidance sources and sensors as well as with the MLS guidance system. The results are thus applicable to both current and future commercial aircraft operations.

MAGNETIC LEADER CABLE

To extend the automatic operations described in the preceding sections through rollout and turnoff, a guidance signal for following a prescribed ground path is required. One potential source of the required guidance information during rollout, turnoff, and taxi is the Magnetic Leader Cable. The cable, or wire, would be in the runway, turnoff, and taxiway along the path which the aircraft is to follow, as in figure 10. An audio frequency current in the cable sets up a magnetic field, which is detected in magnitude and direction by a set of three orthogonal coils mounted in the aircraft. The voltage outputs of the three coils are then amplified, filtered, and detected to produce three varying d.c. voltages V_x, V_y, and V_z which are proportional to the x-, y-, and z- components of the magnetic field. It can be shown theoretically that, assuming the leader cable is an infinitely long straight wire, the ratio of the voltages V_z/V_y is a measure of the lateral displacement y of the coils (and aircraft) from the cable as in figure 11, that is

$$\hat{y}_1 = k_y \, V_z/V_y \tag{7}$$

Similarly, it can be shown that within a small angle approximation the ratio of voltages V_x/V_y is a measure of the aircraft heading ψ relative to the cable, that is,

$$\hat{\psi} = k_\psi \, V_x/V_y \tag{8}$$

A sensor of this type has been investigated analytically and experimentally.

Analytical Studies

Since the current in the cable must have a return path, a practical cable installation would be neither infinite nor straight, but must be some form of closed loop, such as a rectangle. The analytical investigation has emphasized an examination of the effects of a rectangular loop configuration on the sensor performance.

The components of the magnetic field were computed theoretically for various sizes of the loop and for various displacements and headings of an aircraft relative to the cable. The ratios of the components were computed according to equations (7) and (8), and the following results were obtained. The voltage ratio V_z/V_y is no longer a linear function of displacement y as in equation (7). Thus, an exact measure of y would require that the sensor utilize a non-linear calibration curve. Furthermore, the measurement $\hat{\psi}$ is only exact at a point midway between the ends of the loop. However, it may be possible to reduce these effects sufficiently to allow use of the linear relationships by making the rectangular loop large enough such that the return wire is at least 200 meters from the centerline and the ends of the rectangle are at least 200 meters beyond the ends of the runway. Furthermore, errors produced by using a linear calibration become very small near the cable.

Experimental Studies

Tests were conducted using an experimental sensor based on a design by Ohio State University. The processor was designed and fabricated using analog circuits, and the coils were wound on a four-inch wooden cube. For ease and economy of testing, the sensor and support instrumentation were installed in a passenger van modified for this use. An aluminum structure, shown in figure 12, was attached to the rear of the van to support the coils and preamplifier. The processor output signals together with the output of a time code generator were recorded on magnetic tape for post-test data analysis. Tests with the van were conducted at Wallops Flight Center. Leader cables in the form of rectangular loops 305 meters (1,000 ft) long were temporarily installed on various taxiways and runways at Wallops to examine the effects of different runway construction materials on the processor signals.

In general, two types of tests were conducted: static during which the van was stopped at a specified point, and dynamic during which the van was driven along a desired path. For both types, cable current frequencies of 150 Hz, 165 Hz, and 990 Hz were employed, and currents from 0.25 Amperes to 2.0 Amperes were used. Coil heights varied from 1.2 meters (4 ft) to 3.7 meters (12 ft) with most data taken at 2.41 meters (8 feet).

For the dynamic tests the van was driven along the desired path at speeds of approximately 3.6, 8.9, and 22.4 m/sec (8, 20, and 50 mph) with most of the runs being made at 8.9 m/sec. While 8.9 m/sec was somewhat arbitrary, it did afford a compromise among realistic aircraft speed, ability to accurately drive the path, and a desirable data record length in terms of time. Most of the paths were parallel to the cable at displacements from the cable of as much as 21.3 m (70 ft).

The test procedure for each parallel run normally consisted first of recording static data and setting the gains for the paper chart and magnetic tape recorders with the vehicle aligned with the proper parallel mark and at the center of the test area. Then dynamic data was recorded while the van was driven along the selected parallel marker at a constant speed.

Test Results

Plotted in figure 13 is an example of static data taken at Wallops with a cable current of 0.25 A at 990 Hz. The signal V_y and V_z are the d. c. voltages in the y- and z- channels, respectively, after detection. Also shown are the theoretical values computed as part of the analytical studies. As can be seen, the experimental and theoretical data agree quite well. In figure 14 is plotted the corresponding experimental data for the processor $\hat{y}_1$ output, that is, the output obtained by taking the ratio V_z/V_y, as in equation (7). As predicted by the analytical studies of a rectangular loop, the output is a slightly non-linear function of the displacement y. To obtain an accurate measure of displacement, the sensor (or the guidance and control computer) would store and utilize this calibration curve.

In figure 15 is shown a time history plot of dynamic data recorded with the loop installed on the southwest end of taxiway 04/22, part of which is constructed of concrete and part of asphalt. The van was driven at 8.9 m/sec along a path 7.62 m (25 ft) from the cable. The current frequency was again 990 Hz. Using calibration curves, such as the one in figure 14 for $\hat{y}_1$, the data has been converted to engineering units.

Several characteristics of this data are worth noting. First, the $\hat{y}_1$-output is a promising measurement of the displacement y, but the $\hat{\psi}$-output does not accurately measure the heading ψ, which was close to zero for this run. The bias in the heading measurement was judged to be caused, at least in part, by distortion of the magnetic field by the van. In the $\hat{\psi}$ - output there is an obvious ripple which has the same spatial frequency as the sections of concrete and which is apparently caused by the metal reinforcement in the concrete. In both outputs there is a transient near the concrete/asphalt junction, and there is a bias shift of three to four feet in the $\hat{y}_1$-output between the two sections.

Aircraft Tests

To obtain some preliminary data on the effect of the metal aircraft structure and of aircraft electrical systems on sensor performance, limited static tests were conducted using the TCV B-737 aircraft. A magnetic leader cable loop was set up on a taxiway in front of the NASA hangar at LaRC. Static data was taken just as in the van tests with the following exceptions: The coils and pre-amplifier were removed from the van support structure and temporarily installed in one of two locations in the B-737. One of the coil locations was inside the nosecone at a height of about 2.4 m (8 ft), and the other location was below the nosewheel well at a height of .91 m (3 ft). The pre-amplifier was connected via extended cables to the processor and instrumentation in the van. The overall installation can be seen in the photograph in figure 16, and the nosecone installation is shown in figure 17. The aircraft was positioned at the test point using a tug and power to the aircraft electrical systems was supplied by the aircraft APU.

In figure 18 are plotted static $\hat{\psi}$ - output voltage as a function of displacement y for the aircraft oriented at 0^{o} heading and at 5^{o} heading relative to the cable. Due to distortion of the field by the aircraft, the $\hat{\psi}$ - output is a stronger function of y than of ψ at both 150 Hz and 990 Hz. These results were obtained with the coils in the nosecone location. With the coils located below the nosewheel well, the y- dependence is even more dramatic.

The preceding data was taken with no aircraft electrical system operating. Additional static data was taken and the processor outputs were recorded on magnetic tape as various aircraft electrical and avionics systems were turned "on." Analysis of this data indicates that considerable filtering may be required to reduce the interference produced by other avionics, particularly when operating at 990 Hz. Additional tests are required to determine if this filtering is effective.

In summary, the analysis and test results to date indicate that because of the effects of the metal aircraft, an accurate measure of heading probably cannot be obtained with the Magnetic Leader Cable system. However, measurement of lateral displacement from the desired path looks promising. A new experimental sensor suitable for flight test on the B-737 is being designed and fabricated using a combination of analog and digital circuits for increased processing flexibility. Additional tests with the van and then with the aircraft will be conducted to further assess performance and to select such parameter values as the cable frequency and bandpass filter bandwidth.

AUTOMATIC ROLLOUT AND TURNOFF

The automatic rollout and turnoff guidance and control system performs the following tasks: It controls the aircraft from touchdown along the runway centerline and desired high speed turnoff exit, and it decelerates the aircraft to the desired turnoff speed. The basic elements of the system are shown in figure 19 and consist of (1) the filter, (2) the magnetic leader cable processor, and (3) the guidance and control law.

The filter provides estimates of the aircraft position and velocity components in the runway coordinate frame. The inputs to the filter are the MLS measurements of azimuth and range, lateral and longitudinal acceleration, aircraft attitude, and body rates. In simulation studies both a time-varying Kalman filter and a third order complementary filter were used. The Kalman filter and complementary filter were previously designed for use in the automatic approach and landing phases of flight.

The magnetic leader cable processor provides outputs of lateral displacement and relative heading from the cable. These outputs can be provided through either a hardware or software processor given the coil output voltages as inputs.

The guidance and control law is a modified design of the TCV B-737 rollout law which uses the ILS localizer signal for runway centerline location. The modified law consists of two parts--the path tracking law, similar to the localizer law, and a new part, the braking law. Like the localizer law, the modified law commands the rudder and nose wheel positions. In addition, the modified law commands the desired deceleration for input to the autobrake system and the desired nominal reverse thrust.

The inputs to the path tracking law are the position and velocity estimates from the filter, the magnetic leader cable processor outputs, the aircraft heading, and the specified path information (magnetic leader cable location). The law uses these inputs to compute estimates of cross-track error (lateral displacement from the cable), cross-track rate, and heading error. The estimated cross-track error is determined by computing a linear combination of the cross-track error from the filter and the magnetic leader cable processor output. The estimated heading error is a linear combination of relative track angle determined by the filter outputs and heading error from the magnetic leader cable. Using the guidance signals of cross-track error, cross-track rate, and yaw error, the path tracking law determines the commanded rudder and nose wheel positions.

The guidance law also contains a logic section. At touchdown, a determination is made as to whether or not the aircraft can decelerate safely to the desired exit speed using the estimated distance to go, ground speed, and aircraft weight. If the aircraft is unable to decelerate safely, an alternate turnoff exit further down the runway is used in calculating the deceleration profile. When the logic determines that the exit speed is safely achievable, the guidance calculates the total deceleration force necessary to achieve the desired exit speed. If the force is greater than the maximum specified reverse thrust, it sets the commanded reverse thrust to the specified maximum and computes the nominal braking required. If the total force is less than the specified maximum thrust, the reverse thrust is set to slightly less than the total force required and the required nominal braking is computed as previously described. In either case, the reverse thrust command remains constant while the deceleration command to the autobrake system maintains the closed loop control about the desired deceleration. The logic and calculations also take into account wet and dry runway conditions. In addition, the logic triggers computations to estimate the DME bias when crossing over a known position (calibrated position) on the runway. The discrete telling the logic that the calibrated position is being crossed over perhaps could be determined from detecting the magnetic field of a small current driven loop buried in the runway. In the development of this system, this measurement was simulated with an error of 2 to 3 meters.

The braking control law was designed to compute a brake command which would control the aircraft about a desired fixed deceleration, $\ddot{X}_D$, according to the following equation:

$$\ddot{X}_D = \frac{\dot{X}_T^2 - \dot{X}^2}{2\,(d-d_B)}$$

where $\dot{X}_T$ is the desired turnoff speed, $\dot{X}$ is the estimated speed, d is the estimated distance to go to the turnoff or exit, and d_B is the distance before the turnoff at which it is desired to reach the exit speed. This formulation results in a linear decrease in speed. The desired acceleration is then compared with the measured acceleration to determine the acceleration error.

The braking control law integrates the acceleration error and then multiplies the integrator output by a constant gain to compute the command level of braking. At initiation of braking, the auto-brake system is commanded to the nominal braking required in one second. After one second the integrator is initialized and engaged to integrate the acceleration error. The brake command is limited to a constant value for dry runways and to a variable limit for wet runways. The variable limit, which is a function of ground speed, was determined from hydroplane data.

The following summarizes the sequence of events that occur during the automatic rollout and turnoff guidance and control:

- Deploy the ground and speed brakes (spoilers) at main gear compression.
- At two seconds:
  - Compute the nominal reverse thrust and braking if not achievable, recompute the same parameters for the alternate exit.
  - Then initiate the nominal reverse thrust, steering and braking commands.
- Determine DME bias and update position estimates 396 meters (1300 ft) from turnoff
- Deactivate reverse thrust 2.6 m/sec (5 knots) above desired exit speed.
- Continue braking to desired exit speed and turnoff at runway exit.

The performance of the rollout and turnoff system was evaluated using a nonlinear aircraft simulation similar to that described earlier in the DIALS. One addition to the simulation was a model for the landing gear and tire dynamics and preliminary error models for the buried magnetic leader cable signals. The models used for the cable were obtained from the experimental test results described earlier. Figure 20 shows the time histories of four longitudinal parameters--thrust, percent of specified maximum braking, deceleration, and the ground and airspeed. The runway configuration simulated was the Wallop Flight Center (WFC) high speed exit 1158 meters (3800 ft) from threshold - 914 meters (3000 ft) radius. This case was for a dry runway, 5.1 m/sec (10 knot) headwinds and gusts. Note that the braking increases at

first to compensate for the reverse thrust which is lagging the desired command. Also note that as the reverse thrust is reduced to idle, the level of braking increases to compensate. Figure 21 is a time history plot of the aircraft yaw with respect to the runway centerline, the cross-track error from the desired path, and the side acceleration of the aircraft. The cross-track error plot shows the true error, the error measured from the magnetic leader cable, and the error determined from filter estimate. For this run the control system used the cross-track error from the magnetic cable only and the heading error computed only from the filter estimates. The cross-track error plot illustrates that much better accuracy is obtained from the magnetic cable measurement than that computed from the estimates. Note that the lateral acceleration is smooth and that it's slightly greater than .1 g for this 30.9 m/sec (60 knot), 914 m (3000 ft) radius turn. It can be seen that the aircraft reaches its desired turnoff speed just before 15 seconds (see figure 20, percent braking) and begins its turn off the runway about 1 second later as indicated by the yaw plot. Figures 22 and 23 are similar time history plots for a wet runway. Note the lower level of braking as compared to the dry runway case. Also note the longer time it takes to turnoff the wet runway in going to the alternate exit -- approximately 25 seconds. It can be seen from the ground speed trace that the aircraft was decelerated smoothly to its exit speed just before it reached the turn. In both plots (wet and dry) it can be seen that the aircraft tracks the desired path very close during the straight line positions and stands off to the outside of the turns, but within three meters of the desired track.

The simulation results have shown that the automatic guidance and control system provides acceptable performance for both wet and dry runway conditions. In addition, this performance was demonstrated in the presence of aircraft sensor noises and biases, MLS noises and biases, magnetic cable errors modeled from the van tests described earlier and wind disturbances. Further simulation studies still remain to check the performance of the system using a refined landing gear model. These studies should also include tests to determine the effects on performance due to thrust imbalance in the engines.

SUMMARY

Several results have been obtained from a coordinated guidance and control system development effort. The overall objective of the effort is to contribute to the Terminal Configured Vehicle Program goal of increasing terminal area capacity and efficiency, improving approach and landing performance of aircraft in adverse weather conditions, and reducing the aircraft noise perceived on the ground. Using the Microwave Landing System, a magnetic leader cable and airborne sensors as inputs, automatic guidance and control algorithms have been developed for glideslope and localizer acquisition and tracking, flare, rollout and turnoff. In extensive simulation studies, a Digital Integrated Automatic Landing System (DIALS) has demonstrated the capability to perform rapid acquisition of the glideslope and localizer with small overshoots. The DIALS can also accurately track the localizer and preselected glideslopes. This performance and flexibility permits use of short finals and steep noise-abatement approaches. Specific design features

have been incorporated to estimate winds and reduce their effect on performance, to reduce computational requirements, and to produce control maneuvers that should result in pilot acceptance of the design.

Two flare concepts have been developed and evaluated. Flight test results have demonstrated significant reductions in longitudinal touchdown dispersion with reasonable values for sink rate. The flare algorithms have been shown to perform well with either the ILS or MLS landing guidance systems. An advanced rollout and turnoff capability has been developed to complement the precision flare algorithm development in reducing runway occupancy time and thereby increasing airport capacity. A sensor, currently under development, has shown a promise, in both van and limited aircraft tests, of measuring lateral deviation from the desired ground track. A rollout guidance and control system has been developed, using the developmental sensor measurements, to provide acceptable performance for rollout and turnoff under both wet and dry runway conditions. Further simulation studies and flight tests are currently planned for each of the research topics which have been described.

REFERENCES

1. Walsh, T. M.; and Weener, E. F.: Automatic Flight Performance of a Transport Airplane on Complex Microwave Landing System Paths, Presented at the AGARD 25th GCP Symposium on Guidance and Control Design Considerations for Low Altitude and Terminal Area Flight, Dayton, Ohio, October 17-20, 1977.

2. White, W. F.; et al: Flight Demonstrations of Curved Descending Approaches and Automatic Landings, Using Time Referenced Scanning Beam Guidance, NASA TM 78745, May 1978.

3. White, W. F.; and Clark, L. V.: Flight Performance of the TCV B-737 Airplane at Kennedy Airport Using TRSB/MLS Guidance, NASA TM 80148, July 1979.

4. White, W. F.; and Clark, L. V.: Flight Performance of the TCV B-737 Airplane at Jorge Newbery Airport, Buenos Aires, Argentina, Using TRSB/MLS Guidance, NASA TM 80233, January 1980.

5. White, W. F.; and Clark, L. V.: Flight Performance of the TCV B-737 Airplane at Montreal Dorval International Airport, Montreal, Canada, Using TRSB/MLS Guidance, NASA TM 81885, September 1980.

6. Halyo, N.: Development of an Optimal Automatic Control Law and Filter Algorithm for Steep Glideslope Capture and Glideslope Tracking, NASA CR-2720, August 1976.

7. Halyo, N.: Development of a Digital Automatic Control Law for Steep Glideslope Capture and Flare, NASA CR-2834, June 1977.

8. Halyo, N.: Development of a Digital Guidance and Control Law for Steep Approach Automatic Landings Using Modern Control Techniques, NASA CR-3074, February 1979.

9. Staff of Langley Research Center and Boeing Commercial Airplane Company: Terminal Configured Vehicle Program Test Facilities Guide, NASA SP 435, 1980.

10. Lambregts, A. A.; and Creedon, J. F.: Development and Flight Evaluation of Automatic Flare Laws with Improved Touchdown Dispersion, presented at the AIAA Guidance and Control Conference, Danvers, Massachusetts, August 11-13, 1980.

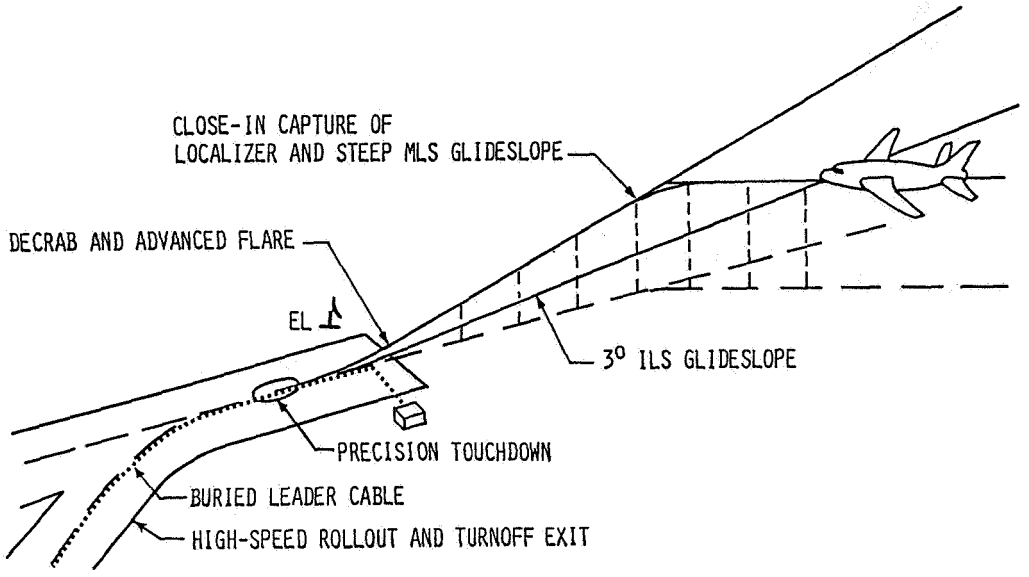

Figure 1.- Pictorial of the DIALS tasks.

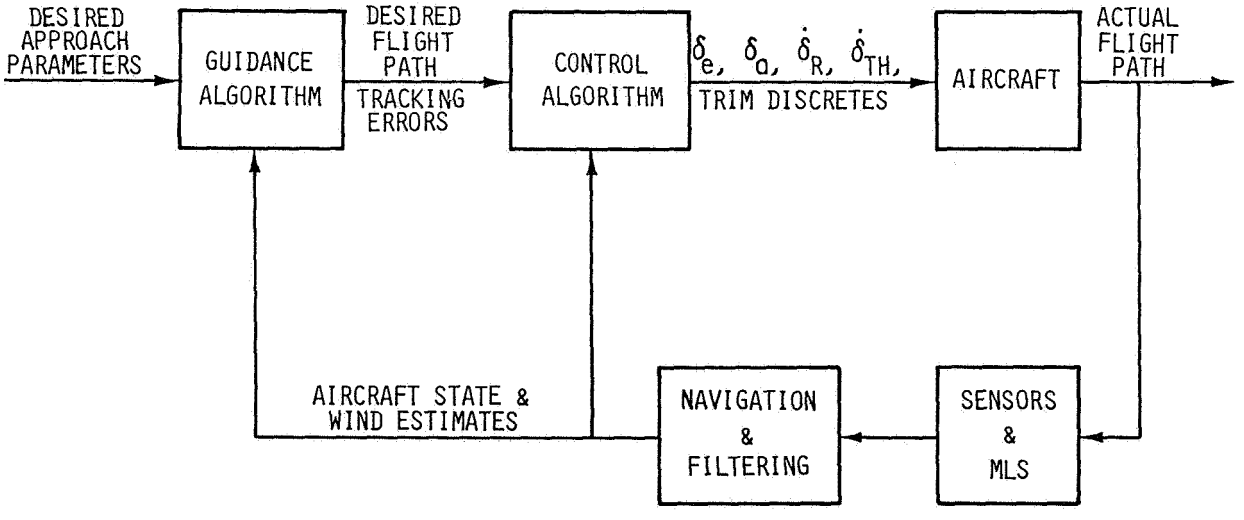

Figure 2.- The DIALS block diagram.

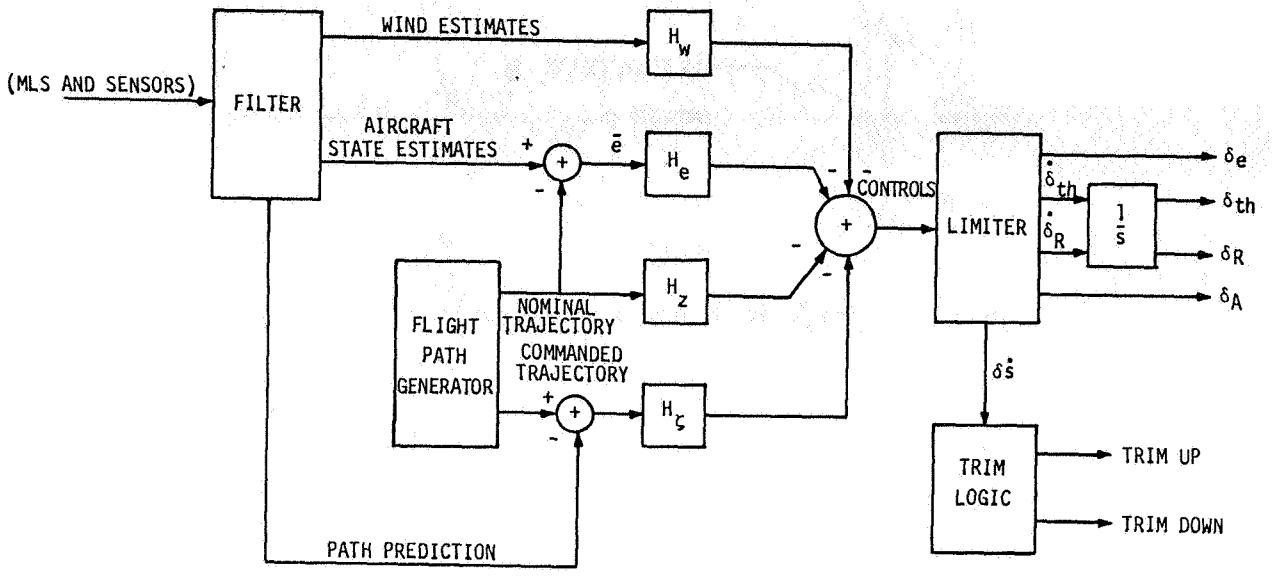

Figure 3.- Block diagram of feedback loop.

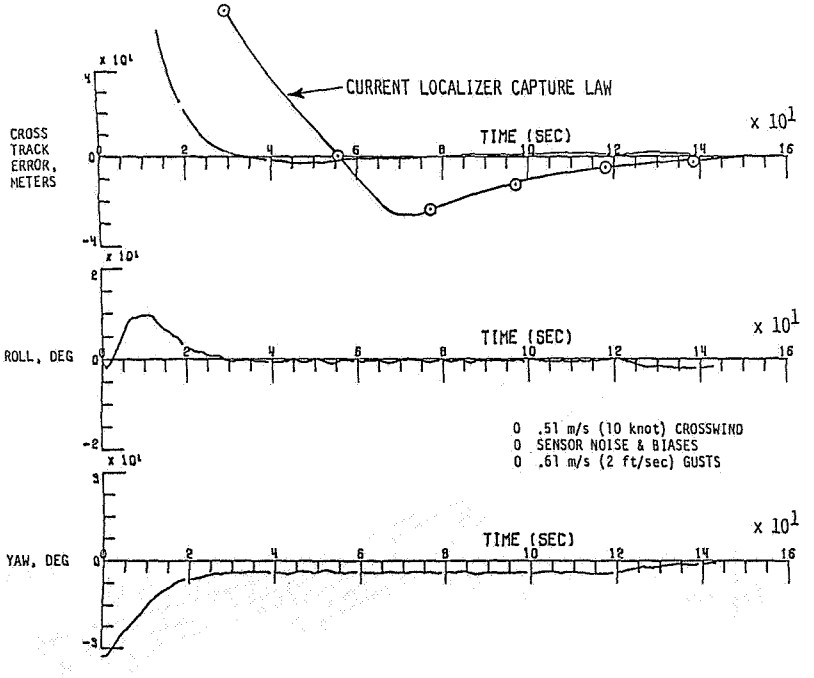

Figure 4.- Capture, track, and decrab of localizer path.

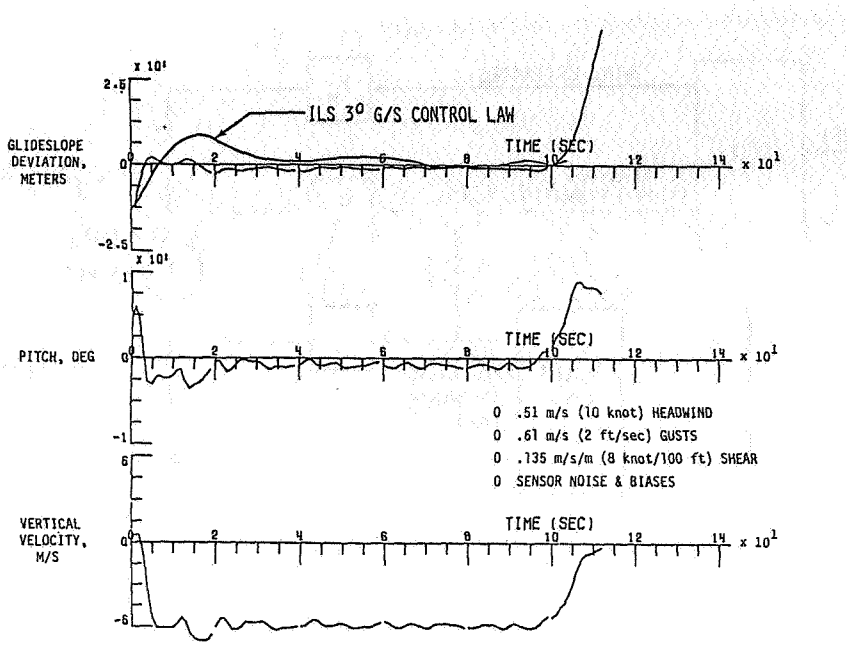

Figure 5.- Capture, track, and flare for 6° glideslope.

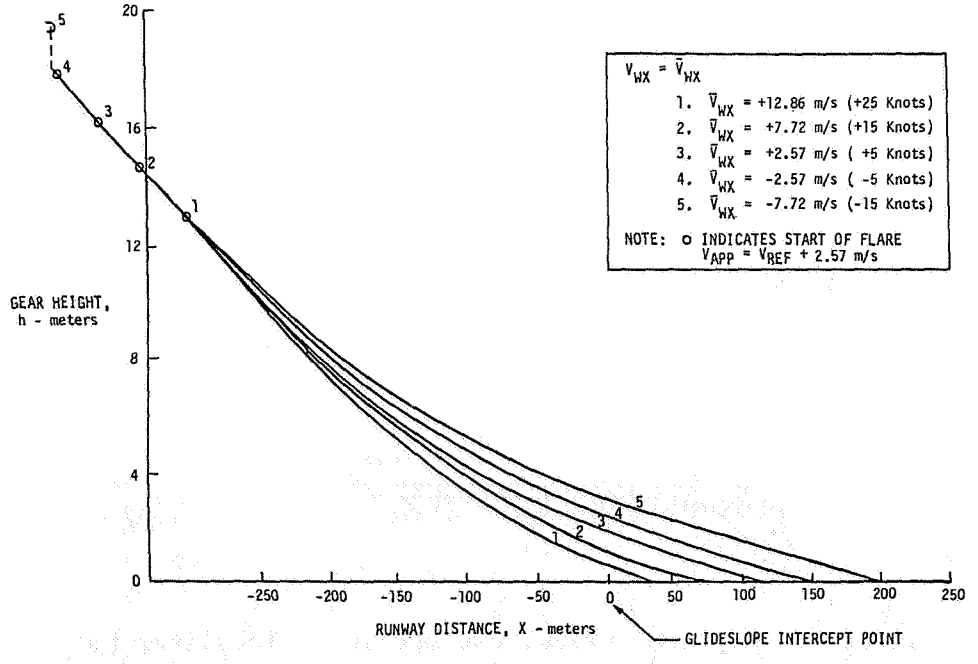

Figure 6.- Variation of $\dot{h}(h)$ flare trajectory with steady state winds.

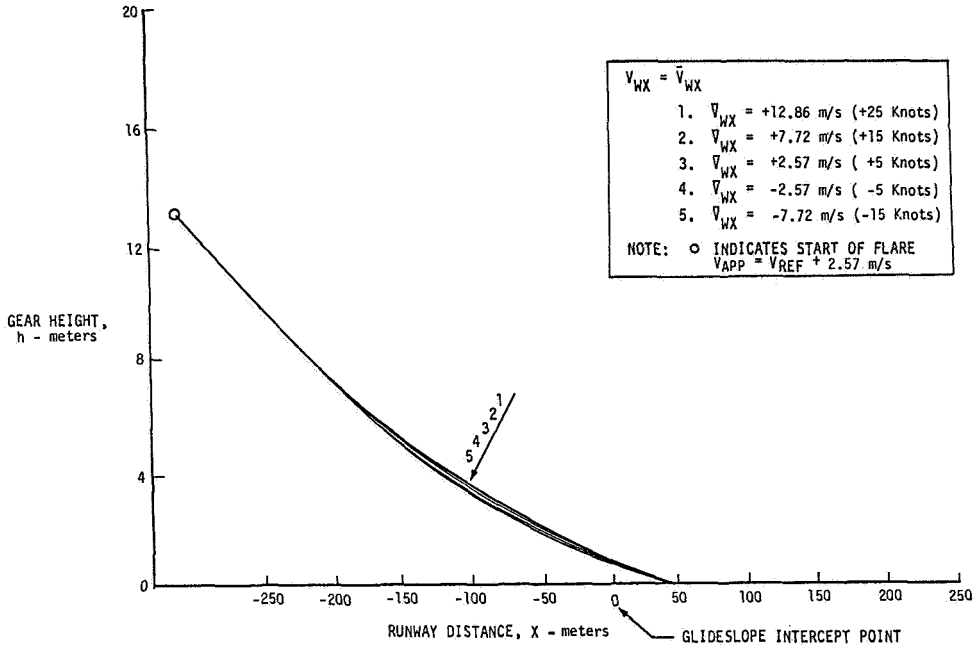

Figure 7.- Variation of $\dot{h}(h,V_G)$ flare trajectory with steady state winds.

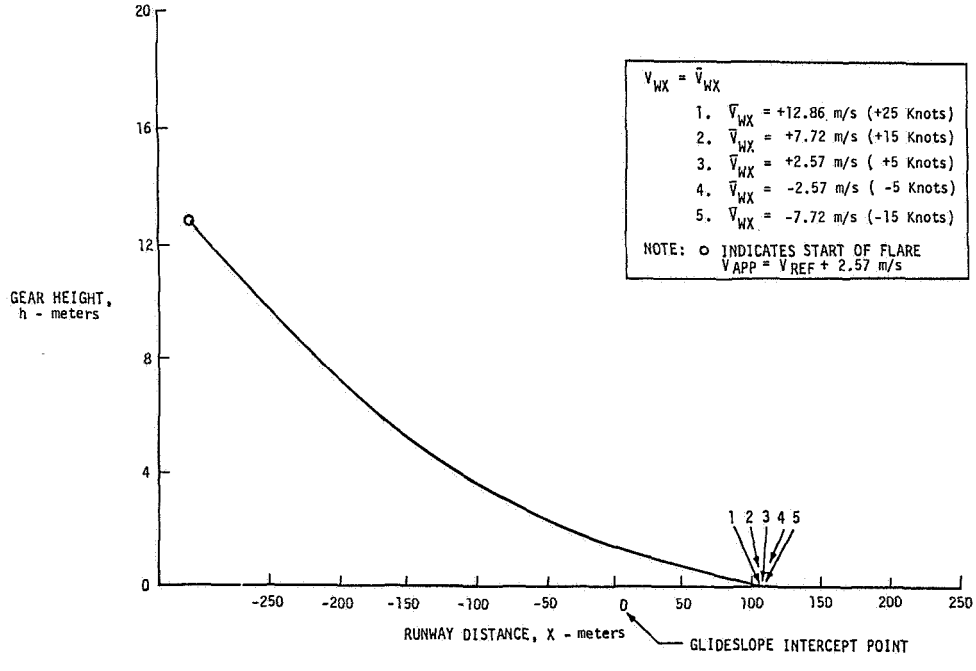

Figure 8.- Variation of $h_1(x)$ flare trajectory with steady state winds.

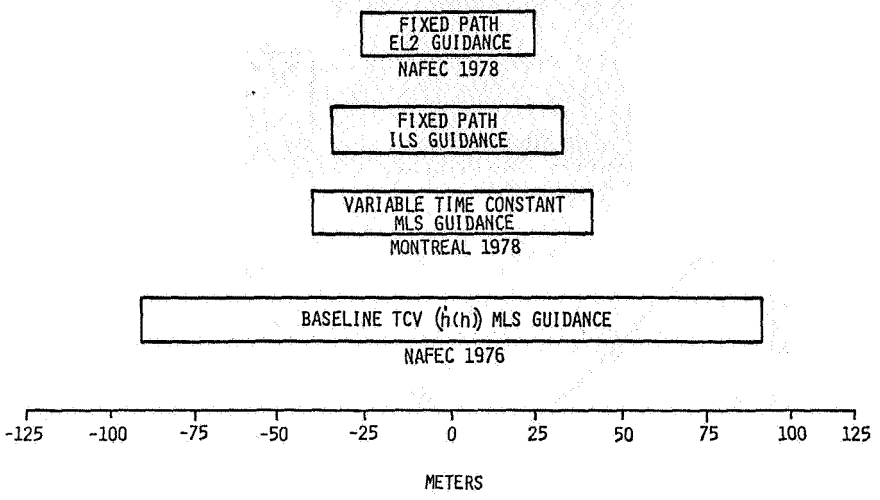

Figure 9.- Flight test ±1σ longitudinal dispersions for the ḣ(h), variable time constant, and fixed path flare laws.

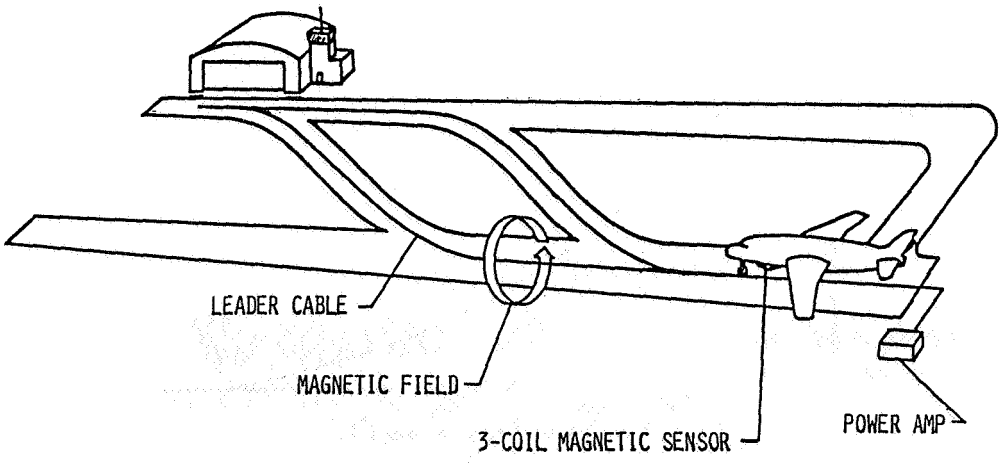

Figure 10.- Magnetic leader cable system.

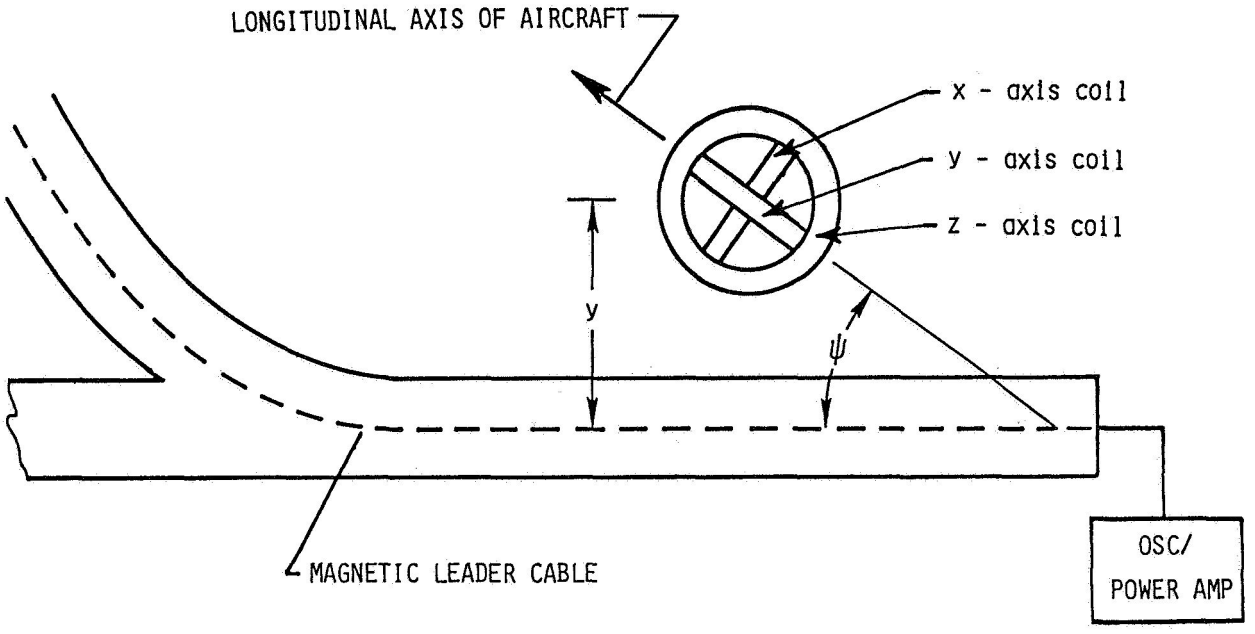

Figure 11.- Displacement and heading of aircraft relative to the cable.

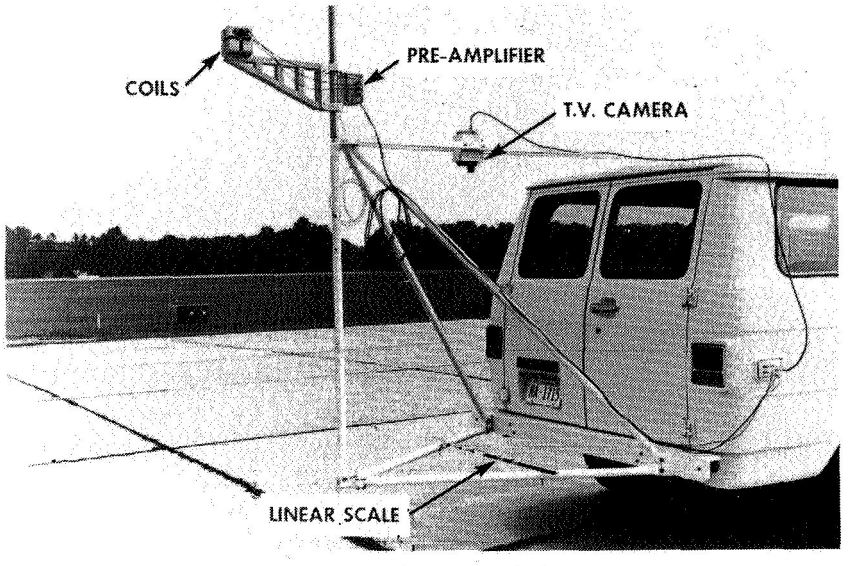

Figure 12.- Van support structure with coils and pre-amplifier.

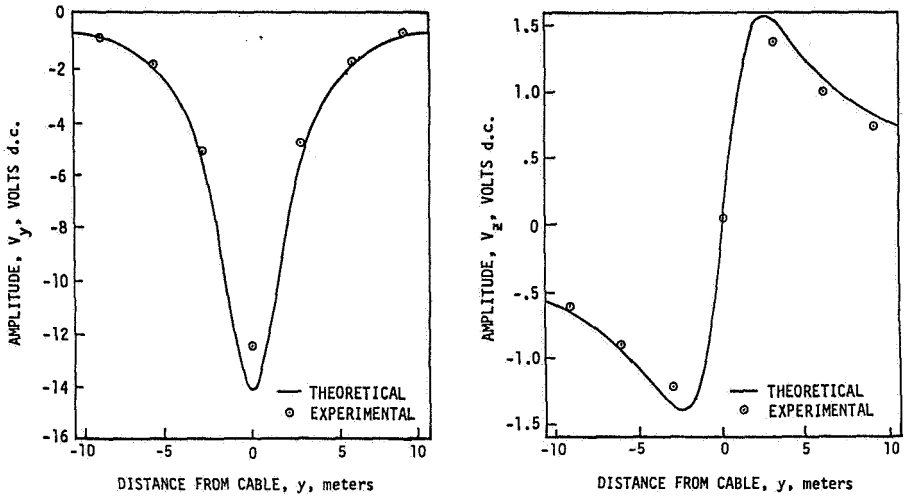

(a) y - channel. (b) z - channel.

Figure 13.- Comparison of theoretical and experimental signal amplitudes.

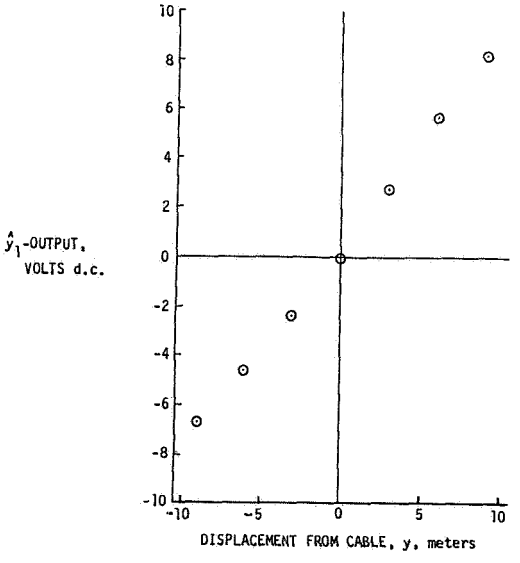

Figure 14.- A typical experimental calibration curve for y_1.

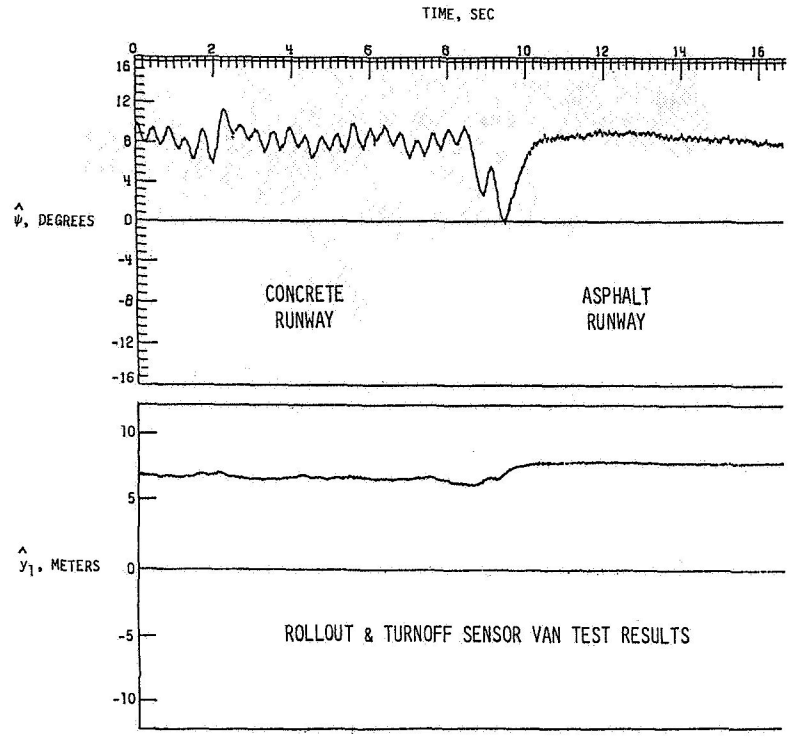

Figure 15.- Time history plot of dynamic data showing effects of taxiway construction material.

Figure 16.- Experimental set-up for aircraft tests.

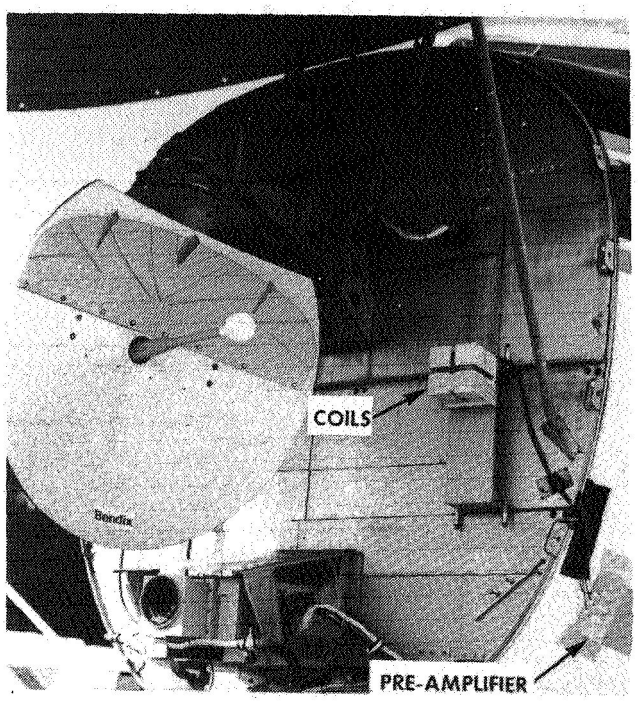

Figure 17.- Sensor location for aircraft tests.

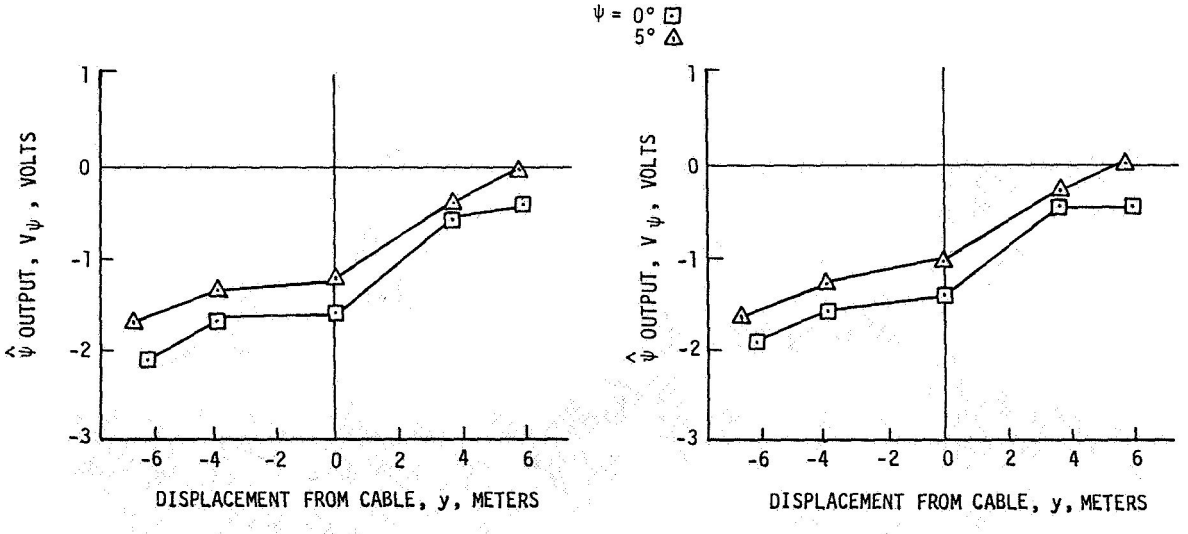

(a) 990 Hz. (b) 150 Hz.

Figure 18.- Static heading data taken with coils in nose of B-737 aircraft.

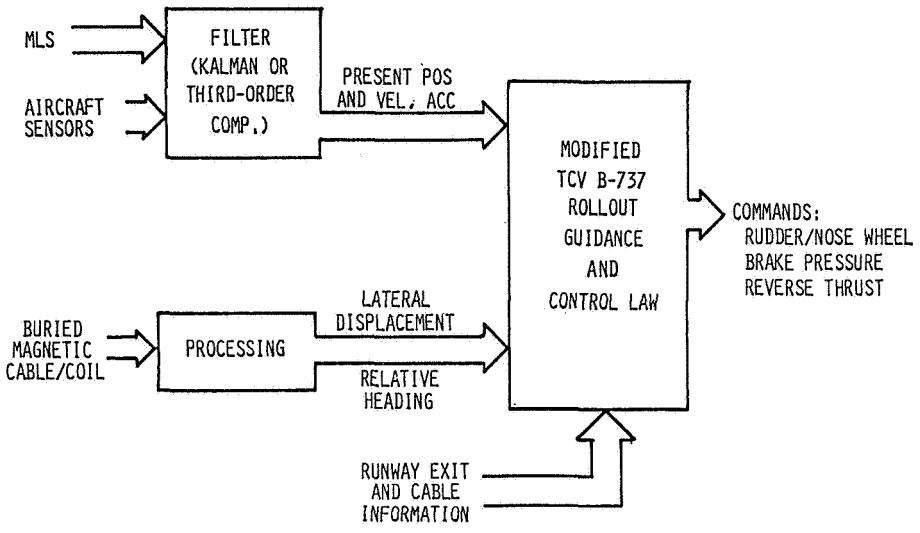

Figure 19.- Automatic rollout and turnoff system.

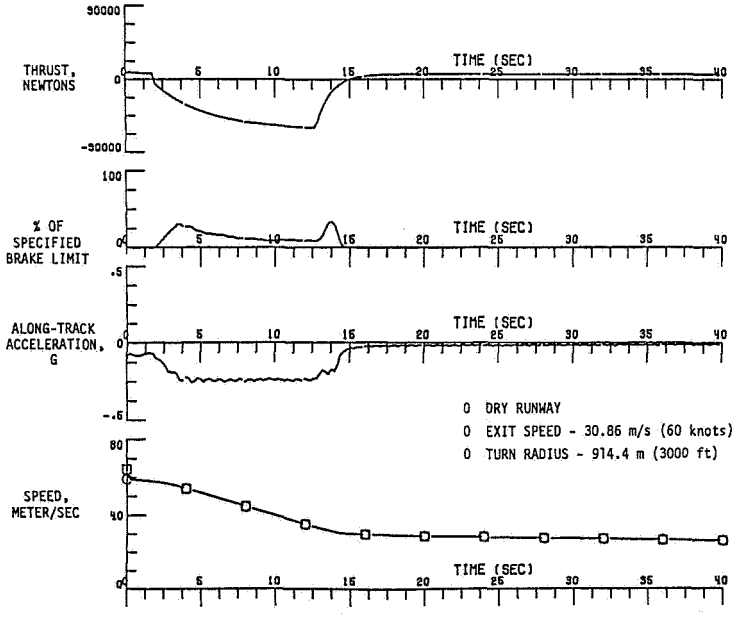

Figure 20.- Automatic rollout and turnoff - longitudinal. Dry runway.

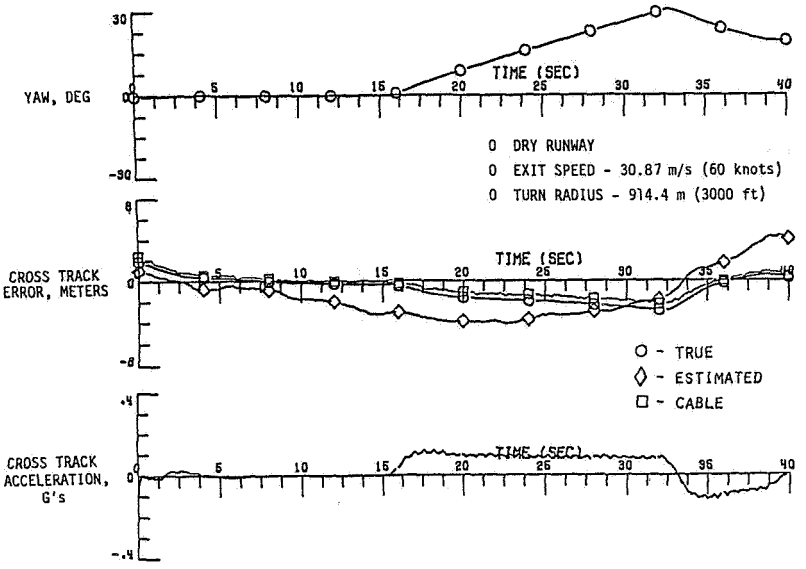

Figure 21.- Automatic rollout and turnoff - lateral. Dry runway.

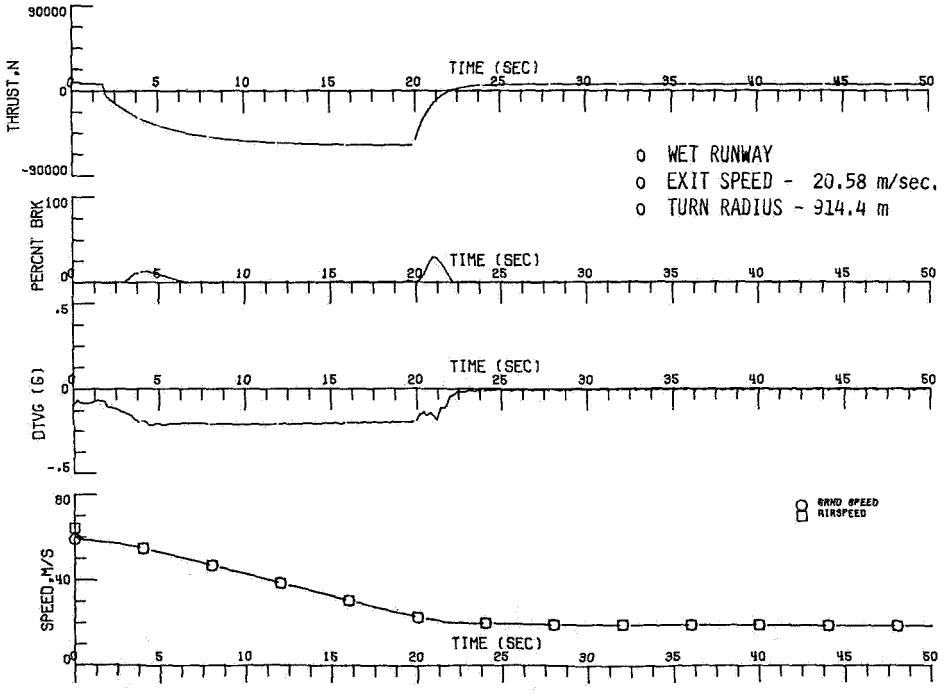

Figure 22.- Automatic rollout and turnoff - longitudinal. Wet runway.

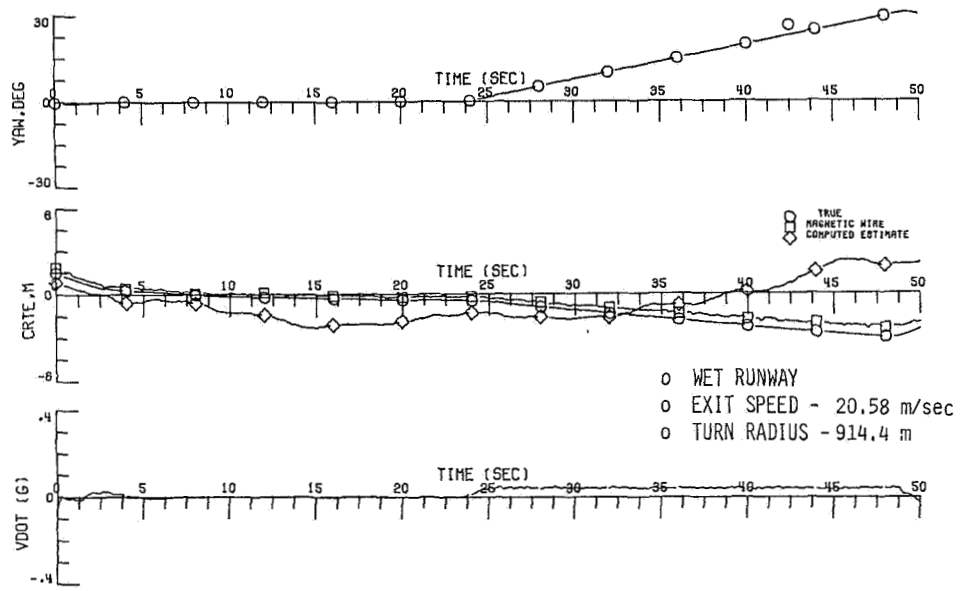

Figure 23.- Automatic rollout and turnoff - lateral. Wet runway.